https://doi.org/10.5194/acp-2020-794
Preprint. Discussion started: 6 August 2020

Atmospheric Chemistry and Physics Discussions

Airborne pollen observations using a multi-wavelength Raman polarization lidar in Finland: characterization of pure pollen types

Xiaoxia Shang[1], Elina Giannakaki[1,2], Stephanie Bohlmann[1], Maria Filioglou[1], Annika Saarto[3], Antti Ruuskanen[1], Ari Leskinen[1,4], Sami Romakkaniemi[1], and Mika Komppula[1]

[1]Finnish Meteorological Institute, Atmospheric Research Centre of Eastern Finland, P.O. Box 1627, 70211, Kuopio, Finland.
[2]Department of Environmental Physics and Meteorology, University of Athens, Athens, Greece.
[3]Aerobiology Unit, University of Turku, Finland.
[4]Department of Applied Physics, University of Eastern Finland, P.O. Box 1627, 70211, Kuopio, Finland

Correspondence to: Xiaoxia Shang (xiaoxia.shang@fmi.fi)

Abstract. We present a novel algorithm for characterizing the optical properties of pure pollen particles, based on the depolarization values obtained in lidar measurements. The algorithm was first tested and validated through a simulator, and then applied to the lidar observations during a four-month pollen campaign from May to August 2016 at the European Aerosol Research Lidar Network (EARLINET) station in Kuopio (62°44'N, 27°33'E), in Eastern Finland. Twenty types of pollen were observed and identified from concurrent measurements with Burkard sampler; Birch (*Betula*), pine (*Pinus*), spruce (*Picea*) and nettle (*Urtica*) pollen were most abundant, contributing more than 90 % of total pollen load, regarding number concentrations. Mean values of lidar-derived optical properties in the pollen layer were retrieved for four intense pollination periods (IPPs). Lidar ratios at both 355 and 532 nm ranged from 55 to 70 sr for all pollen types, without significant wavelength-dependence. Enhanced depolarization ratio was found when there were pollen grains in the atmosphere, and even higher depolarization ratio (with mean values of 25 % or 14 %) was observed with presence of the more non-spherical spruce or pine pollen. The depolarization ratio at 532 nm of pure pollen particles was assessed, resulting to 24 ± 3 % and 36 ± 5 % for birch and pine pollen, respectively. Pollen optical properties at 1064 nm and 355 nm were also estimated. The backscatter-related Ångström exponent between 532 and 1064 nm was assessed as ~0.8 (~0.5) for pure birch (pine) pollen, thus the longer wavelength would be better choice to trace pollen in the air. The pollen depolarization ratio at 355 nm of 17 % and 30 % were found for birch and pine pollen, respectively. The depolarization values show a wavelength dependence for pollen. This can be the key parameter for pollen detection and characterization.

1 Introduction

Pollen has various effects on human health and the environment. The number of people suffering from allergies due to pollen inhalation is rising (Schmidt, 2016). Airborne pollen is recognized as one of the major agents of allergy-related diseases such as asthma, rhinitis, and atopic eczema (Bousquet et al., 2008). Pollen is also biogenic air pollutant which affects both the solar

https://doi.org/10.5194/acp-2020-794
Preprint. Discussion started: 6 August 2020


Atmospheric Chemistry and Physics Discussions

radiation reaching the Earth and cloud optical properties by acting as seed for both cloud droplets and ice crystals (Steiner et al., 2015).

Various networks are built to monitor pollen concentrations at ground level using in situ instruments (Giesecke et al., 2010). In 2020, there is more than 1000 active pollen monitoring stations in the world (Buters et al., 2018, https://oteros.shinyapps.io/pollen_map/, last access: 7 April 2020), with majority based on the Hirst principle (Hirst, 1952). Conventional method of pollen classification is based on pollen morphological characters using microscopy (Holt and Bennett, 2014; Weber, 1998). However, it requires complex procedures for the complete classification and identification, and the results are not publicly available online. Besides, pollen grains can be agile and change their visual nature before the analysis, e.g. undergo an osmotic shock (Miguel et al., 2006), which lead to errors in pollen characterization.

An increasing interest in pollen has arisen in the aerosol lidar community (Noh et al., 2013; Sicard et al., 2016). In our previous study (Bohlmann et al., 2019) we showed on the basis of an 11-day birch pollination period that lidar measurements can detect the presence of pollen grains in the atmosphere, and that the non-spherical pollen grains can generate strong depolarization (we found a mean depolarization ratio of 26 % for the birch-spruce pollen mixture). Therefore, it is possible to observe airborne pollen grains in the atmosphere using depolarization ratio in the absence of other depolarizing non-spherical particles (e.g. dust). We have also reported that lidar derived parameters (e.g. depolarization ratio and Ångström exponent) provide the possibility to identify different pollen types (e.g. birch and spruce pollen). However, the optical properties of pure pollen are still missing due to the fact that the atmospheric aerosol population is always a mixture of several particle types. For instance, the depolarization ratio of pure pollen is an essential parameter needed to separate pollen backscatter from the background aerosol backscatter. Ångström exponent and lidar ratio, which are often used for aerosol typing, are also crucial parameters to be defined for pure pollen particles.

In addition to ground-based lidars, the CALIOP (Cloud-Aerosol LIdar with Orthogonal Polarization) on-board the CALIPSO (Cloud–Aerosol Lidar and Infrared Pathfinder Satellite Observation) provide the vertically-resolved information of atmosphere on a global scale. Currently, CALIPSO aerosol type classification scheme includes seven tropospheric aerosol types (Kim et al., 2018, https://www-calipso.larc.nasa.gov/resources/calipso_users_guide/data_summaries/vfm/index_v420.php, last access: 7 April 2020), in which pollen (or biogenic aerosols in general) is excluded. In that sense, the classification scheme is defective and additional information is needed in order to classify pollen (Sassen, 2008). More detailed ground-based lidar measurements provide the possibility to develop and test such schemes under well characterized conditions, and provides information for a new aerosol type in CALIPSO classification scheme.

In this study, we present a novel method for characterizing the optical properties of pure pollen particles, based on a four months campaign. In Sect. 2, we introduce the pollen campaign and the instruments. In Sect. 3, we present the methodology and the results: Firstly, the pollen information observed by the Burkard sampler and lidar retrieved optical properties for the pollen layer are presented. Secondly, we describe a novel algorithm to estimate the depolarization value for pure pollen. This algorithm is first tested and validated through a simulator in Sect. 3.3 and then applied to the lidar observations in Sect. 3.4. Section 4 is devoted to the summary and conclusion.

https://doi.org/10.5194/acp-2020-794
Preprint. Discussion started: 6 August 2020

Atmospheric Chemistry and Physics Discussions

2 Site and instruments

The measurement campaign was performed from May to August 2016, at the Kuopio station of the European Aerosol Research Lidar Network (EARLINET) in Vehmasmäki (62°44'N, 27°33'E, elevation of 190 m above sea level). This rural site is mainly surrounded by forest, located ~18 km from the city center of Kuopio, in Eastern Finland. Finland provides suitable conditions for the observation of pollen as 78 % of Finland's total area is covered by forests. Airborne *Betula* spp. (birch) pollen is one of the most recognized aeroallergens in northern European countries and the most important cause of pollen allergy (Sofiev et al., 2015; Yli-Panula et al., 2009). The predominant *Betula* species include *B. pendula* and *B. pubescens*, while *B. nana* and *B. pubescens subsp. czerepanovii* can be found in northern parts of the country. As to conifers, *Pinus sylvestris* and *Picea abies* are the most prevalent and *P. sylvestris* pollen typically causes the highest peaks during the pollen season. *P. sylvestris* and *P. abies* are the only naturally growing species of their genre in Finland. Compared to many other European countries, relatively clean background atmospheric conditions in Finland favour pollen detection and further separation of contributions of pollen backscattering from total scattering by using lidars, since there are less other particles, particularly dust, which would complicate the analysis.

The Kuopio station is operated by the Finnish Meteorological Institute, and it is equipped with a ground-based multi-wavelength Raman polarization lidar Polly^{XT} (Engelmann et al., 2016), Doppler lidar, and in-situ instruments next to a 318 m mast (for the meteorological observations) since autumn 2012 (Hirsikko et al., 2014). The cross- and total- polarization channels of the Polly^{XT} allow the retrieval of the volume depolarization ratio (VDR) and linear particle depolarization ratio (PDR) at 532 nm, which provide information on the shape of the scattering particles. Multi-wavelength measurements (355 nm, 532 nm and 1064 nm) enable the determination of Ångström exponents between each wavelength pairs, which are related to the particle nature, mostly the size. During night-time, profiles of extinction and backscatter coefficients at 355 and 532 nm can be derived independently using elastic and inelastic Raman-shifted wavelengths (387 and 607 nm), based on the Raman inversion (Ansmann et al., 1992). The ratio of extinction to backscatter coefficient is called lidar ratio (LR), which is considered an important parameter to separate particle types, as it depends on their single scattering albedo and backscatter phase function, thus being a function of size distribution and chemical composition. In addition to the lidar measurements, a Hirst-type Burkard pollen sampler (Hirst, 1952) was placed 4 meters above ground level (agl) next to the lidar instrument. The Burkard sampler enables identification of pollen types and concentration microscopically with a 2-hour time resolution. More detailed descriptions of the pollen sampler and Polly^{XT} used during this campaign can be found in Bohlmann et al. (2019) and reference therein.

https://doi.org/10.5194/acp-2020-794
Preprint. Discussion started: 6 August 2020


Atmospheric Chemistry and Physics Discussions

3 Methodology and results

3.1 Pollen grain and intense pollination period

During the four months campaign, 20 pollen types were observed and identified from the samples collected with the Burkard sampler. Six from broadleaved trees, observed from end of April to mid of June; three from coniferous trees, with pollination period from mid of May to mid of June; and eleven from grass/weed, observed mainly in July and August. Among them, birch (*Betula*), pine (*Pinus*), spruce (*Picea*) and nettle (*Urtica*) pollen were most abundant, contributing to more than 90 % of the total pollen load, regarding number concentrations. The surrounding forest is mixed in terms of the tree species, but the pollination periods of different dominant pollen types are distinct, as can be seen from the Burkard observed number concentration of specific pollen types shown in Fig. 1a.

Microphotographs of pollen grains for the dominant pollen types are shown in Fig. 1b (photos taken from www.paldat.org, last access: 7 April 2020). Pine and Spruce pollen belong to *Pinaceae* family, which pollinate profusely and greatly contribute to the pollen counts. However, they are rarely considered as allergenic. Their pollen grains are large due to their sacs or bladders, which make them easy to identify. Among winged grains, the body is sub-spheroidal to broadly ellipsoidal. The longest axis (sacci included) of *Pinus sylvestris* (Scots pine) pollen grains is 65-80 µm, while in *Picea abies* (Norway spruce) the axis is longer, 90-110 µm (Nilsson et al., 1977). Birch pollen can cause severe pollinosis, and is recognized as one of the most important allergenic source (D'Amato et al., 2007). Birch pollen grains are sub-oblate to oblate. *B. pubescens* pollen grains are 18-24 × 22-28 µm in size (Nilsson et al., 1977) and *B. pendula* (Silver birch) pollen grains are more or less of the same size (spoken communication from Aerobiology, University of Turku). Nettle is considered moderately allergenic, both in terms of skin tests and amount of exposure to the pollen in the air. Nettle *(Urtica dioica)* pollen grains are oblate-spheroidal to spheroidal, and are quite small with size of 13-17 × 15-20 µm (Nilsson et al., 1977). Information of the dominant pollen types are reported in Table 1, where the pollen season is defined using the 95 % method (Goldberg et al., 1988). The start of the season was defined as the date when 2.5 % of the seasonal cumulative pollen count was trapped and the end of the season when the cumulative pollen count reached 97.5 %.

Four intense pollination periods (IPPs) are defined considering both the pollen seasons of these 4 dominant pollen types (Table 1), and the available lidar measurements. IPP-1 and -2 are selected within the birch pollen season. During IPP-1, almost only birch pollen is observed (97 % contribution in number concentration), while during IPP-2, spruce pollen is additionally present in the air with 14 % contribution. IPP-3 consists of 2 periods within the pine pollen season, separated by a few days with frequent low level clouds (below 1 km) or rain, causing the relatively low pine pollen concentration between these two periods. IPP-4 is defined for nettle pollen study for 3 separate short pollination periods in July and August.

https://doi.org/10.5194/acp-2020-794
Preprint. Discussion started: 6 August 2020


Atmospheric Chemistry and Physics Discussions

3.2 Optical properties of pollen layer

3.2.1 Pollen layer

A pollen layer in the lidar measurements is defined as the lowest observed layer. The layer boundaries are determined using the gradient method (Bösenberg and Matthias, 2003; Flamant et al., 1997; Mattis et al., 2008) based on lidar-derived backscatter coefficient profile at 532 nm wavelength. More detailed description of the layer definition method is described in Bohlmann et al. (2019). Two-hour time averaged lidar profiles are used in this study to match the pollen sampler time resolution. The retrieved pollen layers are shown in Fig. 2a. With an overlap correction applied in this study, the lower limit for reliable backscatter profiles was about 600 m agl. Statistical values of the pollen layer top height agl for the four IPPs were 1.5 ± 0.3 km, 1.3 ± 0.3 km, 1.3 ± 0.4 km, and 1.2 ± 0.3 km, respectively (Fig. 2b). The lowest layer top height was found for the nettle pollen, belonging to herbaceous species. For the relatively larger spruce and pine pollen, the layer top heights were lower compared to the smaller birch pollen.

3.2.2 Lidar-derived optical properties

Mean values of lidar derived optical properties inside the detected pollen layers were retrieved (Table 2); these optical values represent the atmosphere with presence of pollen (thus the mixture of pollen with other aerosols).

Lidar ratio (LR) at 532 nm and LR at 355 nm for pollen layers were retrieved using the standard Raman method (Ansmann et al., 1990) during night-time measurements. The mean values are reported in Table 2, and boxplots of LR at 532 nm and ratio of LRs are shown in Fig. 3(a, b). Although the number of available profiles is limited, our results indicate that pollen are medium to high absorbing particles with values from 55 to 70 sr for all pollen types. For birch dominant IPP-1 and nettle dominant IPP-4, LR of pollen layers at 532 nm is slightly larger than LR at 355 nm. This behaviour is reversed for IPP-3 (pine dominant) and IPP-2 (mixture of birch and spruce). However, no significant wavelength-dependence can be determined on LR values accounting the uncertainties.

The depolarization ratio was clearly enhanced when there were pollen grains in the air, and even higher depolarization ratios were observed with presence of the more non-spherical spruce and pine pollen. Lidar derived PDR values of detected pollen layers for the whole periods of each IPP are shown in Table 2 and Fig. 3c. This indicates the depolarization ratio is the most proper indicator for pollen type. The extinction-related and backscatter-related Ångström exponent were also retrieved for pollen layers. The difference on the Ångström exponent for IPPs is much less evident, as the boxplot of backscatter-related Ångström exponent between 355 and 532 nm shows (Fig. 3d). The use of Ångström exponent to characterize pollen is quite delicate, as its value depends a lot on the background aerosol. Nevertheless, a clear tendency to smaller Ångström exponent with increasing depolarization ratio can be found, as is reported in Bohlmann et al. (2019). Thus under same or similar background conditions, the Ångström exponent can be an indicator for pollen type. Even though we assumed that pollen grains were evenly distributed inside the pollen layer, bigger pollen contribution in the aerosol mixture near the ground was observed.

https://doi.org/10.5194/acp-2020-794
Preprint. Discussion started: 6 August 2020


Atmospheric Chemistry and Physics Discussions

3.3 Simulator

So far, we have retrieved the optical properties of the pollen layers, but the values for pure pollen are still unknown. In this section, we provide an algorithm to estimate the depolarization value for pure pollen particles. This algorithm is first tested through a simulator (Sect. 3.3.2) and then applied to the lidar observations (Sect. 3.4). The simulator includes a direct model and an inverse model modules (the block diagram is shown in Fig. S1 in the supplement); Similar ones have already been used for forest and aerosol studies (Shang et al., 2018; Shang and Chazette, 2015).

3.3.1 Direct model

Two aerosol populations, pollen (depolarizing) and background (non-depolarizing) aerosols, are considered in this simulation. The optical and physical parameters used in the direct calculation are presented in Table 3. The values are based on our lidar measurements or literature (e.g. Illingworth et al., 2015). The *background* here refers to non-depolarized background aerosols (non-pollen particles), which can be polluted continental or biomass burning aerosols. The depolarization ratio at both 355 and 532 nm of non-pollen particle ($\delta_{background}$) are assumed to be 3 %, which is a mean value for pollen-free periods at our measurement site. Pollen grains are quite big and thus can be assumed to be wavelength independent on the backscatter at wavelengths of 355 nm and 532 nm, with the backscatter-related Ångström exponent of 0. Note that these values can be changed freely for the simulation under 2 constraints: i. depolarization ratio of pollen (depolarizing one) should be higher than the depolarization ratio of background aerosol (non-depolarizing one), ii. the values of backscatter-related Ångström exponent for pollen and non-pollen particle should be different.

The extinction coefficient profiles of these two aerosol layers are assumed to following a Gaussian distribution. The optical depth (OD) of the input background aerosol layer is fixed to be 0.1 in this simulation. In order to simulate different pollen contribution to the total aerosol load, we change the pollen load by selecting different input values for the pollen layer OD. Pollen OD is used as 0.002, 0.01, 0.02, 0.05, 0.1, and 1, thus six pollen backscattering are simulated. One example of simulated pollen and background backscatter coefficients is shown in the supplement (Fig. S2a) for pollen OD of 0.1. The pollen layer is defined as the layers below 1 km.

Next, pollen layer and background layer are summed up, and then the vertical profiles of aerosol backscatter coefficient, particle depolarization ratio, lidar ratio and Ångström exponent of the total aerosols are simulated (e.g., Fig. S2b); theoretically, these parameters can be derived directly from lidar observations. In order to keep the consistency of the availability of lidar-derived parameters, particle backscatter coefficient at 532 nm, PDR at 532 nm, and backscatter-related Ångström exponent between 355 and 532 nm simulated for these 6 cases (shown in Fig. 4) will be used later as input of inverse model.

Pollen backscatter contribution (PBC) inside the pollen layer from heights z1 to z2 (in this simulation z1 = 0, z2 = 1 km) is defined as the ratio of pollen backscatter coefficient (β_{pollen}) and the total particle backscatter coefficient ($\beta_{particle}$). Note that the use of "particle" here is to distinguish from "molecular".

https://doi.org/10.5194/acp-2020-794
Preprint. Discussion started: 6 August 2020

Atmospheric Chemistry and Physics Discussions

$$PBC(z1,z2) = \frac{\int_{z1}^{z2} \beta_{pollen}}{\int_{z1}^{z2} \beta_{particle}}, \quad (1)$$

The Ångström exponent (Å) describes the wavelength-dependence on aerosol optical properties (Ångström, 1964). Backscatter-related Å can be expressed as:

$$Å(\lambda_1,\lambda_2) = -\frac{\ln\left(\frac{\beta(\lambda_1)}{\beta(\lambda_2)}\right)}{\ln\left(\frac{\lambda_1}{\lambda_2}\right)} \quad (2)$$

In this section λ_1 and λ_2 are 355 and 532 nm, respectively.

We investigate here the relationship of Å and PBC of the pollen layer. In order to simplify the calculation, we introduce a parameter η, which is defined as:

$$\eta = \left(\frac{355}{532}\right)^{-Å} \quad (3)$$

Where Å is the backscatter-related Ångström exponent between 355 and 532 nm, for the total particle backscatter. The PBC at 532 nm is inversely proportional to this parameter η. Using the previous 6 simulated cases, a perfect linear relationship is found to fit the η versus PBC (Fig. 5).

3.3.2 Inverse model

In this section, we provide a novel method and develop an inverse model to estimate the depolarization ratio of pure pollen particles. Tesche et al. (2009) provide a method to separate dust and non-dust contributions, based on the difference of the depolarization ratio values of these two types. This separation method is applied here to separate the 2 simulated aerosol types. Lidar-derived particle depolarization ratio ($\delta_{particle}$) can be expressed as the ratio of cross- ($\beta^{\perp}$) and parallel- ($\beta^{/\!/}$) polarized particle backscatter coefficient:

$$\delta_{particle} = \frac{\beta^{\perp}_{pollen} + \beta^{\perp}_{background}}{\beta^{/\!/}_{pollen} + \beta^{/\!/}_{background}}, \quad (4)$$

The particle backscatter coefficient $\beta_{particle}$ is the sum of cross- and parallel-polarized particle backscatter coefficient of both pollen and background aerosols:

$$\beta_{particle} = \beta^{\perp}_{pollen} + \beta^{\perp}_{background} + \beta^{/\!/}_{pollen} + \beta^{/\!/}_{background}, \quad (5)$$

The pollen backscatter coefficient can be thus separated from the total particle backscatter coefficient, expressed as:

$$\beta_{pollen} = \beta_{particle} \frac{(\delta_{particle} - \delta_{background})(1 + \delta_{pollen})}{(\delta_{pollen} - \delta_{background})(1 + \delta_{particle})}, \quad (6)$$

The only remaining unknown to solve the Eq.6 is the depolarization ratio for pure pollen (δ_{pollen}). Next we use previously simulated $\beta_{particle}$ and $\delta_{particle}$, and the assumed $\delta_{background}$.

In the first step, the depolarization ratio for pure pollen was assumed to be several different values (e.g., 10%, 20%, 30%, 40%, 50%), denoted as δ_x, in the simulator. Related pollen backscatter contribution (PBC) inside the pollen layer, can be retrieved (Eq.1). As its value depends on the assumed pollen depolarization (δ_x), it can be expressed as PBC_{δ_x}.

https://doi.org/10.5194/acp-2020-794
Preprint. Discussion started: 6 August 2020


Atmospheric Chemistry and Physics Discussions

Mean values of backscatter-related Ångström exponent between 355 and 532 nm inside the pollen layer, denoted as Å, were also retrieved. The relationship of Å and PBC was investigated using the parameter η (Eq.3). Scatter plots using mean values of η and PBC_{δ_x} in the pollen layer for different cases are shown in Fig. 6. For these relationships, perfect linear fits (linear regression relationship) can be found and plotted as dotted lines in the Fig. 6, following the equation:

$$\hat{\eta}(PBC_{\delta_x}) = a_1 \cdot PBC_{\delta_x} + a_0, \quad (7)$$

The fitting coefficient (a_1, a_0) values to determine the estimated parameter $\hat{\eta}$ vary for different assumed values of δ_x. Theoretically, for each linear fit equation, PBC_{δ_x} values can range from 0 to 1, with 0 meaning no pollen and 1 meaning 100 % pollen in the observed aerosol particle population. Therefore, for each assumed δ_x, the $\hat{\eta}$ value for PBC_{δ_x}=1 can be defined as the value for the pure pollen, and denote as $\hat{\eta}(1_{\delta_x})$.

In Sect. 3.3.1, we made an assumption that the backscatter-related Ångström exponent between 355 and 532 nm of pure pollen (denoted as $Å_{pollen}$) is 0 as input, which results in a value of 1 for the parameter η. In this simulation, we assumed the same values ($\hat{Å}_{pollen}$=0); the goal was thus to find the value of 1 for $\hat{\eta}(1_{\delta_x})$. From previous results shown in Fig. 6, we can see a δ_x between 30 % to 40 % may result in a $\hat{\eta}(1_{\delta_x})$=1 (the black triangle in Fig. 6).

Hence, in the second step, more δ_x values between that range (30 % - 40 %) were used in the simulation, and one can retrieve the relative value of $\hat{\eta}(1_{\delta_x})$ for each case. These values are presented in Fig. 7. For these data, a good linear fit can be found with high correlation coefficients ~-1.

Finally, in the third step, under the assumption of $\hat{Å}_{pollen}$=0, pollen depolarization ratio of 35 % was found, resulting in a $\hat{\eta}(1_{\delta_x})$=1 (shown by the black triangle in Fig. 7). This result is exactly the same as the input value of the direct model, which validates the algorithm and provides the feasibility of using this inverse model to retrieve the pure pollen depolarization ratio values. A detailed flow chart of this inverse model is given in Fig. 8. Note that the initial values of δ_x in both step 1 and 2 can be chosen freely, for values bigger than background depolarization ratio and smaller than 100 %. This method can also be applied to other two aerosol types (e.g., dust and non-dust aerosols), under the condition that the depolarization ratio of one aerosol type is the only unknown parameter, and other parameters are known or can be assumed.

3.3.3 Uncertainty study

The uncertainty study of this method is investigated in this section, using the parameters of previous simulated 6 cases (Sect. 3.3.1).

Under the ideal condition, which means there is no noise on the input profiles for the inverse model, the depolarization ratio of pollen (depolarizing one) can be retrieved perfectly as long as the value is higher than the depolarization ratio of background aerosol (non- depolarizing one). δ_{pollen} of 0.04 has been tested, and the correct value was successful retrieved. Note that for this case, the assumed values of δ_x for the first step should be selected as lower values (e.g. 0.032, 0.05, 0.1, 0.2). The more values of δ_x used in the first and second steps of the inverse model, the better precision will be for the results, but also longer

https://doi.org/10.5194/acp-2020-794
Preprint. Discussion started: 6 August 2020


Atmospheric Chemistry and Physics Discussions

computation time is needed. It is also possible to combine the first and second steps of inverse model, by using many assumed values of δ_x (e.g. 0.032, 0.033, 0.034, …, 0.98, 0.99) for the first step, at the cost of long computation time.

In the second and third steps of the inverse model, we assumed that the backscatter-related Ångström exponent between 355 and 532 nm of pure pollen (denoted as $\hat{\mathring{A}}_{pollen}$) is 0, which was the input value of direct model. But in the reality, such information is not always available. Under different assumed values of $\hat{\mathring{A}}_{pollen}$, there will be a bias on the estimated values of pollen depolarization ratio. For example, if we assume $\hat{\mathring{A}}_{pollen}$ is 0.5 (i.e., the parameter $\hat{\eta}_{pollen}$ is 1.22) in the inverse model, the estimated pollen depolarization ratio is found to be 0.31 in Fig. 7, with a bias of -0.04. The uncertainty due to different assumed $\hat{\mathring{A}}_{pollen}$ were simulated (show in Fig. S3), for assumed $\hat{\mathring{A}}_{pollen}$=0 ±0.5, relative uncertainties were assessed as ~15 %.

Further on, we investigate the random uncertainty due to the noise on input lidar profiles, using the simulator based on a Monte Carlo approach. The parameters for previous simulated 6 cases (Sect. 3.3.1) are again used in this simulation, but noises are additionally added, considering normal statistical distributions, which are introduced by a normal random generator (Fig. S1). The PDR and Å are calculated from particle backscatter coefficients, so we only need to apply different noise levels to the particle backscatter coefficients in the direct model, and related PDR and Å with noise can be retrieved. To simplify the problem, the initial noise levels for both backscatter coefficients at 355 and 532 nm were considered under the same assumptions. We defined "1 group" as 1 draw of 6 simulated backscatter profiles with a certain noise level; these 6 backscatter profiles are with pollen OD of 0.002, 0.01, 0.02, 0.05, 0.1, and 1. For each statistical simulation, we used 200 draws (i.e. 200 groups of profiles). This uncertainty study was investigated by 2 parts:

i. Fix input pollen depolarization ratio, and change noise levels. We used 0.35 as the input pollen depolarization ratio. In case of taking 10 % as the noise level on the backscatter coefficients, one group of 6 simulated profiles with noise are shown in Fig. 9. Pollen depolarization ratio of 0.346 was found for this group using the inverse model, with a bias of -0.004 compared to the input value of 0.35. Similarly, pollen depolarization ratio values were retrieved for each of the 200 generated groups. These 200 values had a mean value of 0.351 ± 0.005, thus an uncertainty of 0.005 (relative uncertainty of 1.4 %) was found. We changed the noise levels (e.g., 1 %, 10 %, 20 %, 40 %, and 60 %) on the backscatter coefficients by the normal random generator, and 200 draws were performed for each statistical simulation under each noise level. The uncertainties of the retrieved pollen depolarization ratio against the noise levels were assessed and shown in Fig. 10a.

ii. Fix noise level and change input pollen depolarization ratio. In the second simulation, we keep 10 % as the noise level on the backscatter, and change the input pollen depolarization ratio values as 0.1, 0.2, 0.3, 0.4, and 0.5. Under each assumption, 200 draw were performed to derive the uncertainties values, which are reported in Fig. 10b. Relative uncertainties on retrieved pollen depolarization ratio of 0.4 % to 1.7 % were found.

From simulation results, small uncertainty and good accuracy were found using this algorithm. Nevertheless, even with the introduced noise levels, these simulations were still performed under quasi ideal condition. For each simulated group, 6 cases were used to provide a wide range of values of PBCs (from ~0.01 to ~0.9), which leading good constraints to find a fitting line for the regression relationship of PBC and η (e.g. Fig. 6). If only 3 cases (with Pollen OD of 0.01, 0.02, and 0.05) were used

https://doi.org/10.5194/acp-2020-794
Preprint. Discussion started: 6 August 2020


Atmospheric Chemistry and Physics Discussions

for each group, 2 to 4 times bigger uncertainties were found. It is hard to give qualitative values for such uncertainty study, but the wider range of PBC values are in the data set, the better the retrievals will be. The vertical resolution used here was 30 m (as the raw resolution of our lidar); and increasing the vertical resolution of the lidar would result in smaller uncertainty in simulation.

3.4 Estimation of optical properties for pure pollen from lidar observations

3.4.1 Pollen optical properties at 532 nm

The inverse model was applied to the real lidar observations in this section to retrieve the depolarization ratio for pure pollen. We assume that there are only pollen and non-depolarized background aerosols in the air, which is reasonable because of the clean aerosol conditions at the measurement site.

For the first step, the depolarization ratio of pure pollen (δ_x) was assumed to be 20%, 30%, 40%, or 50%, and the depolarization ratio of non-pollen particles ($\delta_{background}$) was assumed to be 3 %. Under each assumption, we calculated the pollen backscatter coefficient during every IPPs, and thus extract the related pollen backscatter contribution (PBC) inside the pollen layer (PBC_{δ_x}). Mean values of backscatter-related Ångström exponents between 355 and 532 nm inside the pollen layer were retrieved and denoted as Å. The relationship of Å and PBC_{δ_x} of pollen layers in each IPP was investigated using the parameter η (Eq.3). Two examples are shown in Fig. 11: (a) the scatter plot using mean η and PBC_{δ_x} for IPP-1, here the pollen depolarization ratio was assumed to be 20 %; (b) similar plot for IPP-3, here the pollen depolarization ratio of 40 % was assumed. Similar scatter plots under different values of assumed δ_x (20%, 30%, 40%, or 50%) are given in the supplement (Fig. S4 for IPP-1 and in Fig. S5 for IPP-3).

Based on results from the first step, in the second step of the inverse model, more δ_x values between 20 %-30 % for IPP-1 (between 30 %-40 % for IPP-3) were used for the calculations. Linear fitting lines were generated for the $\hat{\eta}$ and PBC_{δ_x} (Eq. 7) under each assumed δ_x. For these fitting lines, the $\hat{\eta}$ value for PBC_{δ_x}=1 was retrieved, denoted as $\hat{\eta}(1_{\delta_x})$ and reported in Fig. 12. $\hat{\eta}(1_{\delta_x})$ presents the $\hat{\eta}$ values when the pollen contribution in the observed aerosol particle population is 100%. Using these estimated $\hat{\eta}(1_{\delta_x})$ and δ_x, linear fits (shown by dotted lines in Fig. 12) can be assessed with high correlations.

Further on for the third step, δ_x value which results in a certain value of $\hat{\eta}(1_{\delta_x})$ could be assumed as the depolarization ratio value of pure pollen. Under the assumption that the backscatter-related Ångström exponent between 355 and 532 nm of pure pollen (denoted as $Å_{pollen}$) is 0 (i.e. $\hat{\eta}(1_{\delta_x})$=1), depolarization ratio of 24 % or 36 % were found for IPP-1 or IPP-3, respectively, which are related to the pure birch or pure pine pollen (Table 4). There is no values of Ångström exponent for pure pollen in the literature, but this assumption ($Å_{pollen}$= 0) is almost realistic, as pollen grains are quite big, and thus can be assumed to be wavelength independent on the backscatter at wavelengths of 355 nm and 532 nm. For big particles as dust, Mamouri and Ansmann (2014) reported Ångström exponent between 440 and 675 nm with values of -0.2 for coarse dust and 0.25 for total dust.

https://doi.org/10.5194/acp-2020-794
Preprint. Discussion started: 6 August 2020


Atmospheric Chemistry and Physics Discussions

Uncertainty study was investigated based on method describe in Sect. 3.3.3 using a Monte Carlo approach. The overall relative uncertainties of the lidar-derived backscatter coefficients are of the order of 5 %–10% (Baars et al., 2012), we took 10 % here in the simulation. Initial pollen depolarization ratio values were selected as 24 % for birch and 36 % for pine for the uncertainty simulation. Based on the lidar observations (Fig. 11, Fig. S4 and S5), the simulated cases were selected so that the PBC values range from 2 % to 70 % for birch and 2 % to 90 % for pine. The initial input $Å_{pollen}$ was selected as 0 and assumed $\hat{Å}_{pollen}$ ranged from -0.5 and 0.5. Estimated uncertainties (shown in Fig. S6) were found as 12 % for birch and 14 % for pine (Table 4). Note that the different initial input values of $Å_{pollen}$ may introduce additional bias. If we assume the true value of $Å_{pollen}$ is between -0.5 to 0.5 (i.e. values of $\hat{\eta}$ from 0.82 to 1.22, shown by red dotted lines in Fig. 12), depolarization ratios of 19 % to 27 % can be found for birch pollen, and 26 % to 44 % can be found for pine pollen. The optical properties of pure pollen is lacking in the literature. Cao et al. (2010) measured the linear depolarization ratio of different pollen types in an aerosol chamber, by disseminating 2 g of the selected pollen; They determined a linear depolarization ratio at 532 nm for paper birch of 33 %, and for Virginia pine of 41 %. These values are higher than what we retrieved in this study, but it has to be kept in mind that these two experiments have been conducted in quite different environments and conditions.

The retrieval of depolarization ratios for pure spruce or pure nettle pollen was not possible with this dataset. During IPP-2, there was always a mixture of birch and spruce pollen with variable mixing rate; in addition, the number of available measurements is limited. For nettle pollen, we have observed relatively small depolarization ratio values, together with a small variation, which makes the separation more challenging.

3.4.2 Pollen optical properties at 1064 nm and 355 nm

Similar study was performed to investigate the relationship between backscatter-related Ångström exponent between 532 and 1064 nm and pollen backscatter contribution at 532 nm, here we introduce another parameter η':

$$\eta' = \left(\frac{1064}{532}\right)^{-Å'} \quad (8)$$

Where $Å'$ is the backscatter-related Ångström exponent between 532 and 1064 nm, for the total particle backscattering. From the earlier simulations, we found out that the pollen backscatter contribution at 532 nm is proportional to this parameter η'.

The inverse model was applied for several assumed pollen depolarization ratios at 532 nm (ranging from 0.2 to 0.6), and no values of $\hat{\eta'}$=1 (i.e. $\hat{Å}'_{pollen}$=0) was found (Fig. S7). This result may due to the fact that the laser beam at longer wavelengths would be more sensitive to bigger particles (pollen). Thus, there is some wavelength dependence on the backscattering between 532 and 1064 nm.

Considering the previously estimated depolarization ratios at 532 nm for pure birch (pine) pollen of 24 % (36 %), the related η' was found to be 0.58 (0.69), corresponding to the value of ~0.8 (~0.5) for the backscatter-related Ångström exponent between 532 and 1064 nm.

https://doi.org/10.5194/acp-2020-794
Preprint. Discussion started: 6 August 2020


Atmospheric Chemistry and Physics Discussions

Depolarization ratio at 355 nm can be also estimated, as pollen backscatter at both 355 and 532 nm should be the same under the assumption that the backscatter-related Ångström exponent between 355 and 532 nm for pure pollen is 0. Pollen backscatter contribution at 355 nm ($PBC_{\delta_x,355}$) was calculated using lidar-derived particle backscatter coefficient at 355 nm. The inverse model was applied here for the backscatter-related Ångström exponent between 355 and 532 nm and pollen backscatter contribution at 355 nm, using a third parameter η'':

$$\eta'' = \left(\frac{532}{355}\right)^{-Å} \quad (9)$$

η'' is proportional to the pollen backscatter contribution at 355 nm. Here Å is the backscatter-related Ångström exponent between 355 and 532 nm, for the total particle backscattering. Under different values of assumed pollen depolarization ratio at 355 nm ($\delta_{x,355}$) from 0.1 to 0.4, linear correlations were found for η'' and $PBC_{\delta_x,355}$ (Fig. S8). Values for $\widehat{\eta''}(1_{\delta_x,355})$ for 100 % pollen backscatter contribution at 355 nm are reported in Fig. 13, against related $\delta_{x,355}$. Finally, the pollen depolarization ratios at 355 nm of 17 % and 30 % were found for IPP-1 (birch) and IPP-3 (pine), respectively (Table 4). Cao et al. (2010) found smaller values with a linear depolarization ratio at 355 nm for paper birch of 8 %, and for Virginia pine of 20 %.

The particle depolarization ratio at 355 nm can be calculated by using the pollen depolarization ratio at 355 nm. Mean values of depolarization ratio of pollen layers for IPP-1 and IPP-3 were retrieved and shown in Fig. 14. For both periods, PDR at 355 nm values are relatively smaller than the ones at 532 nm.

Uncertainty values for pollen depolarization ratios and particle depolarization ratio at 355 nm are not given in this paper, as these estimations were under the assumption that the backscatter-related Ångström exponent between 355 and 532 nm for pure pollen is 0, and base on previously retrieved pollen depolarization ratios at 532 nm. More uncertainty sources should be considered for the uncertainty study, and it is complicated to give qualitative values. Nevertheless, a wavelength dependence seems to be found for depolarization values when pollen is present, which may be a key parameter for pollen recognition and characterization. Thus, depolarization ratio at different wavelengths are needed to identify different pollen types.

4 Summary and conclusions

We have defined lidar-derived properties for pure pollen based on a four months pollen campaign, which was performed during May to August 2016 in Kuopio station in Eastern Finland. This station is part of the European Aerosol Research Lidar Network (EARLINET). Twenty types of pollen were observed and identified by Burkard sampler; among which, birch (*Betula*), pine (*Pinus*), spruce (*Picea*) and nettle (*Urtica*) pollen are most abundant, contributing more than 90 % of total pollen load, regarding number concentrations. Four intense pollination periods (IPPs) were defined considering both the pollen seasons and the available lidar measurements.

Mean values of lidar-derived optical properties in the pollen layer were used to characterise pollen for each IPP. We found that lidar ratio (LR) values range from 55 to 70 sr for all pollen types, indicating that pollen is medium to high absorbing

https://doi.org/10.5194/acp-2020-794
Preprint. Discussion started: 6 August 2020


Atmospheric Chemistry and Physics Discussions

particles. No significant wavelength-dependence could be determined on LR values using LR at 355 nm and 532 nm, regarding the uncertainties. The wide range of LRs suggest that the LR alone is not a suitable parameter to discriminate between different pollen types. Nonetheless, we showed that the depolarization ratio is the most proper indicator for pollen and further the pollen type, as the depolarization ratio was enhanced when there were pollen in the air, and even higher depolarization ratio was observed with presence of the more non-spherical spruce and pine pollen. The Ångström exponent could be used to classify different pollen types only under same or similar background conditions, as its value depends a lot on the background aerosols. As the main results, we provide a novel method for the characterization of pure pollen particles. We present an algorithm to estimate the depolarization values for pure pollen, under the assumption that backscatter-related Ångström exponent between 355 and 532 nm should be zero for pure pollen, as pollen grain are quite large and can be assumed to be wavelength independent at these 2 wavelengths. This algorithm was first tested and validated through a simulator (including a direct model and an inverse model modules). It was applied to the lidar observations; the depolarization ratio at 532 nm of pure pollen particles was assessed, resulting to 24 % ± 3 % and 36 % ± 5 % for birch and pine pollen, respectively. Pollen optical properties at 1064 nm and 355 nm were also estimated base on retrieved pollen depolarization ratio at 532 nm. The pollen depolarization ratio at 355 nm of 17 % and 30 % were found for birch and pine pollen, respectively. The depolarization values show a wavelength dependence for pollen. This can be the key parameter for pollen detection and characterization. Also, a wavelength dependence on the backscatter between 532 and 1064 nm was found, with the value of the backscatter-related Ångström exponent between 532 and 1064 nm of ~0.8 (~0.5) for pure birch (pine) pollen. Based on simulations in this study, we found that depolarization ratios at 355 nm and 1064 nm would provide valuable information for pollen study, thus more multi-wavelength lidar studies with depolarization characterization on atmospheric pollen are necessary. The presented novel algorithm and the estimated optical properties for pure pollen in this study, provide a good method for pollen characterization and classification. Such ground-based lidar measurements also provide the possibility to implement a new aerosol type to the CALIPSO classification scheme, for example using the depolarization ratio at 532 nm.

Data availability. Lidar data are available upon request from the authors and data "quicklooks" are available on the PollyNET website (http://polly.tropos.de/, last access: 25 June 2020).

Author Contributions. XS analysed the data, developed the algorithm and the simulator, and wrote the paper. XS, EG, MK, and SR conceptualized and finalized the methodology. XS and SB performed the lidar data analysis. AS analyzed the pollen samples. MK and EG initiated and managed the project. MF, AR, AL, and MK participated in the measurement campaign. All authors were involved in the paper editing, interpretation of the results and discussion of the manuscript.

Conflicts of Interest. The authors declare no conflict of interest.

https://doi.org/10.5194/acp-2020-794
Preprint. Discussion started: 6 August 2020

Atmospheric Chemistry and Physics Discussions

Special issue statement. This article is part of the special issue "EARLINET aerosol profiling: contributions to atmospheric and climate research". It is not associated with a conference.

Acknowledgments. The authors would like to thank the use of the microphotographs of pollen grains, from PalDat (PalDat – a palynological database, 2000 onwards, www.paldat.org, last access: 7 April 2020), courtesy of the Division of Structural and Functional Botany, University of Vienna. Elina Giannakaki acknowledge the support of Hellenic Foundation for Research and Innovation (H.F.R.I.) under the "First Call for H.F.R.I. Research Projects to support Faculty members and Researchers and the procurement of high-cost research equipment grant (Project number: 2544).

Financial support. This work was supported by the Academy of Finland (projects no. 310312 and 329216).

References

Ångström, A.: The parameters of atmospheric turbidity, Tellus A, 16, 64–75, doi:10.3402/tellusa.v16i1.8885, 1964.

Ansmann, A., Riebesell, M. and Weitkamp, C.: Measurement of atmospheric aerosol extinction profiles with a Raman lidar., Opt. Lett., 15(13), 746–748, doi:10.1364/OL.15.000746, 1990.

Ansmann, A., Wandinger, U., Riebesell, M., Weitkamp, C. and Michaelis, W.: Independent measurement of extinction and backscatter profiles in cirrus clouds by using a combined Raman elastic-backscatter lidar, Appl. Opt., 31, 7113–7131, 1992.

Baars, H., Ansmann, A., Althausen, D., Engelmann, R., Heese, B., Müller, D., Artaxo, P., Paixao, M., Pauliquevis, T. and Souza, R.: Aerosol profiling with lidar in the Amazon Basin during the wet and dry season, J. Geophys. Res. Atmos., 117(D21), D21201, doi:10.1029/2012JD018338, 2012.

Bohlmann, S., Shang, X., Giannakaki, E., Filioglou, M., Saarto, A., Romakkaniemi, S. and Komppula, M.: Detection and characterization of birch pollen in the atmosphere using multi-wavelength Raman lidar in Finland, Atmos. Chem. Phys. Discuss., 14559–14569, doi:10.5194/acp-2019-635, 2019.

Bösenberg, J. and Matthias, V.: EARLINET: A European Aerosol Research Lidar Network to Establish an Aerosol Climatology., MPI Rep., 348, 6–31, 2003.

Bousquet, J., Khaltaev, N., Cruz, A. A., Denburg, J., Fokkens, W. J., Togias, A., Zuberbier, T., Baena-Cagnani, C. E., Canonica, G. W., Van Weel, C., Agache, I., Aït-Khaled, N., Bachert, C., Blaiss, M. S., Bonini, S., Boulet, L.-P., Bousquet, P.-J., Camargos, P., Carlsen, K.-H., Chen, Y., Custovic, A., Dahl, R., Demoly, P., Douagui, H., Durham, S. R., Van Wijk, R. G., Kalayci, O., Kaliner, M. A., Kim, Y.-Y., Kowalski, M. L., Kuna, P., Le, L. T. T., Lemiere, C., Li, J., Lockey, R. F., Mavale-Manuel, S., Meltzer, E. O., Mohammad, Y., Mullol, J., Naclerio, R., O'Hehir, R. E., Ohta, K., Ouedraogo, S., Palkonen, S., Papadopoulos, N., Passalacqua, G., Pawankar, R., Popov, T. A., Rabe, K. F., Rosado-Pinto, J., Scadding, G. K., Simons, F. E. R., Toskala, E., Valovirta, E., Van Cauwenberge, P., Wang, D.-Y., Wickman, M., Yawn, B. P., Yorgancioglu, A., Yusuf, O. M., Zar, H., Annesi-Maesano, I., Bateman, E. D., Kheder, A. Ben, Boakye, D. A., Bouchard, J., Burney, P., Busse, W. W.,

Chan-Yeung, M., Chavannes, N. H., Chuchalin, A., Dolen, W. K., Emuzyte, R., Grouse, L., Humbert, M., Jackson, C., Johnston, S. L., Keith, P. K., Kemp, J. P., Klossek, J.-M., Larenas-Linnemann, D., Lipworth, B., Malo, J.-L., Marshall, G. D., Naspitz, C., Nekam, K., Niggemann, B., Nizankowska-Mogilnicka, E., Okamoto, Y., Orru, M. P., Potter, P., Price, D., Stoloff, S. W., Vandenplas, O., Viegi, G. and Williams, D.: Allergic Rhinitis and its Impact on Asthma (ARIA) 2008*, Allergy, 63(s86), 8–160, doi:10.1111/j.1398-9995.2007.01620.x, 2008.

Buters, J. T. M., Antunes, C., Galveias, A., Bergmann, K. C., Thibaudon, M., Galán, C., Schmidt-Weber, C. and Oteros, J.: Pollen and spore monitoring in the world, Clin. Transl. Allergy, 8(1), 9, doi:10.1186/s13601-018-0197-8, 2018.

Cao, X., Roy, G. and Bernier, R.: Lidar polarization discrimination of bioaerosols, Opt. Eng., 49(11), 116201, doi:10.1117/1.3505877, 2010.

D'Amato, G., Cecchi, L., Bonini, S., Nunes, C., Annesi-Maesano, I., Behrendt, H., Liccardi, G., Popov, T. and van Cauwenberge, P.: Allergenic pollen and pollen allergy in Europe, Allergy, 62(9), 976—990, doi:10.1111/j.1398-9995.2007.01393.x, 2007.

Engelmann, R., Kanitz, T., Baars, H., Heese, B., Althausen, D., Skupin, A., Wandinger, U., Komppula, M., Stachlewska, I. S., Amiridis, V., Marinou, E., Mattis, I., Linné, H. and Ansmann, A.: The automated multiwavelength Raman polarization and water-vapor lidar PollyXT: the neXT generation, Atmos. Meas. Tech., 9(4), 1767–1784, doi:10.5194/amt-9-1767-2016, 2016.

Flamant, C., Pelon, J., Flamant, P. H. and Durand, P.: Lidar determination of the entrainment zone thickness at the top of the unstable marine atmospheric boundary layer, Boundary-Layer Meteorol., 83(2), 247–284, doi:10.1023/A:1000258318944, 1997.

Giesecke, T., Fontana, S. L., van der Knaap, W. O., Pardoe, H. S. and Pidek, I. A.: From early pollen trapping experiments to the Pollen Monitoring Programme, Veg. Hist. Archaeobot., 19(4), 247–258, doi:10.1007/s00334-010-0261-3, 2010.

Goldberg, C., Buch, H., Moseholm, L. and Weeke, E. R.: Airborne Pollen Records in Denmark, 1977--1986, Grana, 27(3), 209–217, doi:10.1080/00173138809428928, 1988.

Hirsikko, A., O'Connor, E. J., Komppula, M., Korhonen, K., Pfüller, A., Giannakaki, E., Wood, C. R., Bauer-Pfundstein, M., Poikonen, A., Karppinen, T., Lonka, H., Kurri, M., Heinonen, J., Moisseev, D., Asmi, E., Aaltonen, V., Nordbo, A., Rodriguez, E., Lihavainen, H., Laaksonen, A., Lehtinen, K. E. J., Laurila, T., Petäjä, T., Kulmala, M. and Viisanen, Y.: Observing wind, aerosol particles, cloud and precipitation: Finland's new ground-based remote-sensing network, Atmos. Meas. Tech., 7(5), 1351–1375, doi:10.5194/amt-7-1351-2014, 2014.

Hirst, J. M.: An automatic volumetric spore trap, Ann. Appl. Biol., 39(2), 257–265, doi:10.1111/j.1744-7348.1952.tb00904.x, 1952.

Holt, K. A. and Bennett, K. D.: Principles and methods for automated palynology, New Phytol., 203(3), 735–742, doi:10.1111/nph.12848, 2014.

Illingworth, A. J., Barker, H. W., Beljaars, A., Ceccaldi, M., Chepfer, H., Clerbaux, N., Cole, J., Delanoë, J., Domenech, C., Donovan, D. P., Fukuda, S., Hirakata, M., Hogan, R. J., Huenerbein, A., Kollias, P., Kubota, T., Nakajima, T., Nakajima, T. Y., Nishizawa, T., Ohno, Y., Okamoto, H., Oki, R., Sato, K., Satoh, M., Shephard, M. W., Velázquez-Blázquez, A.,

Wandinger, U., Wehr, T., van Zadelhoff, G.-J., Illingworth, A. J., Barker, H. W., Beljaars, A., Ceccaldi, M., Chepfer, H., Clerbaux, N., Cole, J., Delanoë, J., Domenech, C., Donovan, D. P., Fukuda, S., Hirakata, M., Hogan, R. J., Huenerbein, A., Kollias, P., Kubota, T., Nakajima, T., Nakajima, T. Y., Nishizawa, T., Ohno, Y., Okamoto, H., Oki, R., Sato, K., Satoh, M., Shephard, M. W., Velázquez-Blázquez, A., Wandinger, U., Wehr, T. and Zadelhoff, G.-J. van: The EarthCARE Satellite: The Next Step Forward in Global Measurements of Clouds, Aerosols, Precipitation, and Radiation, Bull. Am. Meteorol. Soc., 96(8), 1311–1332, doi:10.1175/BAMS-D-12-00227.1, 2015.

Kim, M.-H., Omar, A. H., Tackett, J. L., Vaughan, M. A., Winker, D. M., Trepte, C. R., Hu, Y., Liu, Z., Poole, L. R., Pitts, M. C., Kar, J. and Magill, B. E.: The CALIPSO version 4 automated aerosol classification and lidar ratio selection algorithm, Atmos. Meas. Tech., 11(11), 6107–6135, doi:10.5194/amt-11-6107-2018, 2018.

Mamouri, R. E. and Ansmann, A.: Fine and coarse dust separation with polarization lidar, Atmos. Meas. Tech., 7(11), 3717–3735, doi:10.5194/amt-7-3717-2014, 2014.

Mattis, I., Müller, D., Ansmann, A., Wandinger, U., Preißler, J., Seifert, P. and Tesche, M.: Ten years of multiwavelength Raman lidar observations of free-tropospheric aerosol layers over central Europe: Geometrical properties and annual cycle, J. Geophys. Res., 113, D20202, doi:10.1029/2007JD009636, 2008.

Miguel, A. G., Taylor, P. E., House, J., Glovsky, M. M. and Flagan, R. C.: Meteorological Influences on Respirable Fragment Release from Chinese Elm Pollen, Aerosol Sci. Technol., 40(9), 690–696, doi:10.1080/02786820600798869, 2006.

Nilsson, S. T. (Siwert T., Praglowski, J. and Nilsson, L.: Atlas of airborne pollen grains and spores in northern Europe, Natur o. kultur. [online] Available from: https://agris.fao.org/agris-search/search.do?recordID=SE7801026 (Accessed 17 June 2020), 1977.

Noh, Y. M., Lee, H., Müller, D., Lee, K., Shin, D., Shin, S., Choi, T. J., Choi, Y. J. and Kim, K. R.: Investigation of the diurnal pattern of the vertical distribution of pollen in the lower troposphere using LIDAR, Atmos. Chem. Phys., 13(15), 7619–7629, doi:10.5194/acp-13-7619-2013, 2013.

Sassen, K.: Boreal tree pollen sensed by polarization lidar: Depolarizing biogenic chaff, Geophys. Res. Lett., 35(18), L18810, doi:10.1029/2008GL035085, 2008.

Schmidt, C. W.: Pollen Overload: Seasonal Allergies in a Changing Climate, Environ. Health Perspect., 124(4), A70–A75, doi:10.1289/ehp.124-A70, 2016.

Shang, X. and Chazette, P.: End-to-end simulation for a forest-dedicated full-waveform lidar onboard a satellite initialized from airborne ultraviolet lidar experiments, Remote Sens., 7(5), doi:10.3390/rs70505222, 2015.

Shang, X., Chazette, P. and Totems, J.: Analysis of a warehouse fire smoke plume over Paris with an N2 Raman lidar and an optical thickness matching algorithm, Atmos. Meas. Tech., 11(12), doi:10.5194/amt-11-6525-2018, 2018.

Sicard, M., Izquierdo, R., Alarcón, M., Belmonte, J., Comerón, A. and Baldasano, J. M.: Near-surface and columnar measurements with a micro pulse lidar of atmospheric pollen in Barcelona, Spain, Atmos. Chem. Phys., 16(11), 6805–6821, doi:10.5194/acp-16-6805-2016, 2016.

Sofiev, M., Berger, U., Prank, M., Vira, J., Arteta, J., Belmonte, J., Bergmann, K.-C., Chéroux, F., Elbern, H., Friese, E.,

https://doi.org/10.5194/acp-2020-794
Preprint. Discussion started: 6 August 2020


Atmospheric Chemistry and Physics Discussions

Galan, C., Gehrig, R., Khvorostyanov, D., Kranenburg, R., Kumar, U., Marécal, V., Meleux, F., Menut, L., Pessi, A.-M., Robertson, L., Ritenberga, O., Rodinkova, V., Saarto, A., Segers, A., Severova, E., Sauliene, I., Siljamo, P., Steensen, B. M., Teinemaa, E., Thibaudon, M. and Peuch, V.-H.: MACC regional multi-model ensemble simulations of birch pollen dispersion in Europe, Atmos. Chem. Phys., 15(14), 8115–8130, doi:10.5194/acp-15-8115-2015, 2015.

Steiner, A. L., Brooks, S. D., Deng, C., Thornton, D. C. O., Pendleton, M. W. and Bryant, V.: Pollen as atmospheric cloud condensation nuclei, Geophys. Res. Lett., 42(9), 3596–3602, doi:10.1002/2015GL064060, 2015.

Tesche, M., Ansmann, A., Müller, D., Althausen, D., Engelmann, R., Freudenthaler, V. and Groß~, S.: Vertically resolved separation of dust and smoke over Cape Verde using multiwavelength Raman and polarization lidars during Saharan Mineral Dust Experiment 2008, J. Geophys. Res., 114, D13202, doi:10.1029/2009JD011862, 2009.

Weber, R. W.: Pollen Identification, Ann. Allergy, Asthma Immunol., 80(2), 141–148, doi:10.1016/S1081-1206(10)62947-X, 1998.

Yli-Panula, E., Fekedulegn, D. B., Green, B. J. and Ranta, H.: Analysis of Airborne Betula Pollen in Finland; a 31-Year Perspective, Int. J. Environ. Res. Public Health, 6(6), 1706–1723, doi:10.3390/ijerph6061706, 2009.

https://doi.org/10.5194/acp-2020-794
Preprint. Discussion started: 6 August 2020

Atmospheric Chemistry and Physics Discussions

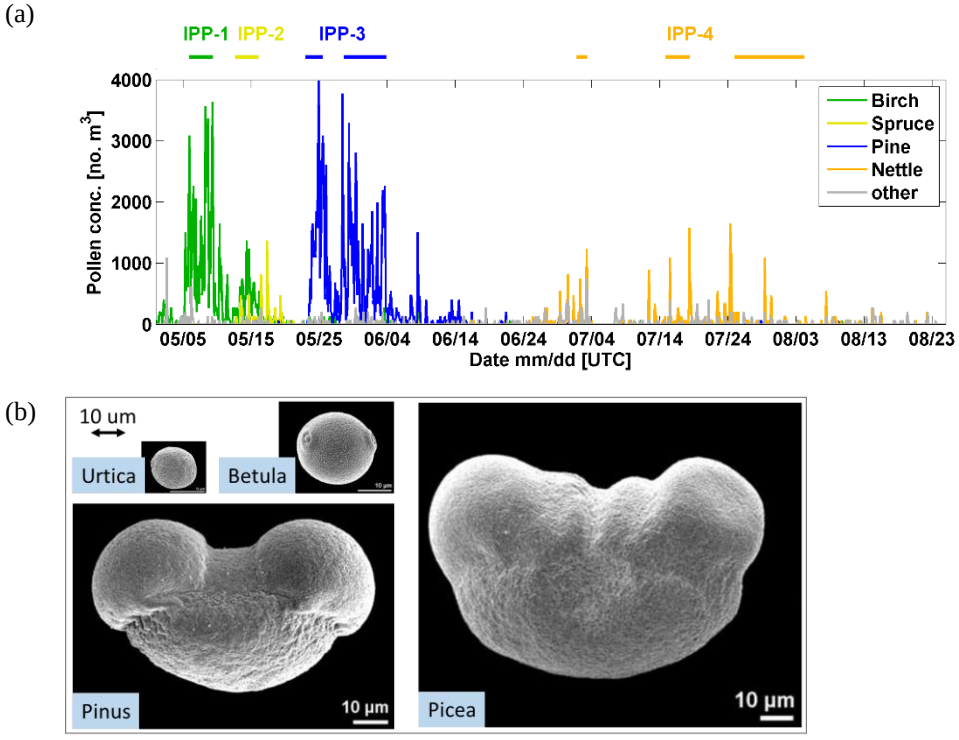

Figure 1. (a) Pollen concentration (2-hour average) measured by the Burkard sampler at roof level. The main pollen types are shown by colours. Defined intense pollination periods (IPPs) are shown by lines on the top. (b) Microphotographs of pollen grain: *Urtica* (nettle pollen), *Betula pendula* (birch pollen), *Pinus* (pine pollen), *Picea abies* (spruce pollen). Source: PalDat – a palynological database (www.paldat.org, last access: 7 April 2020).

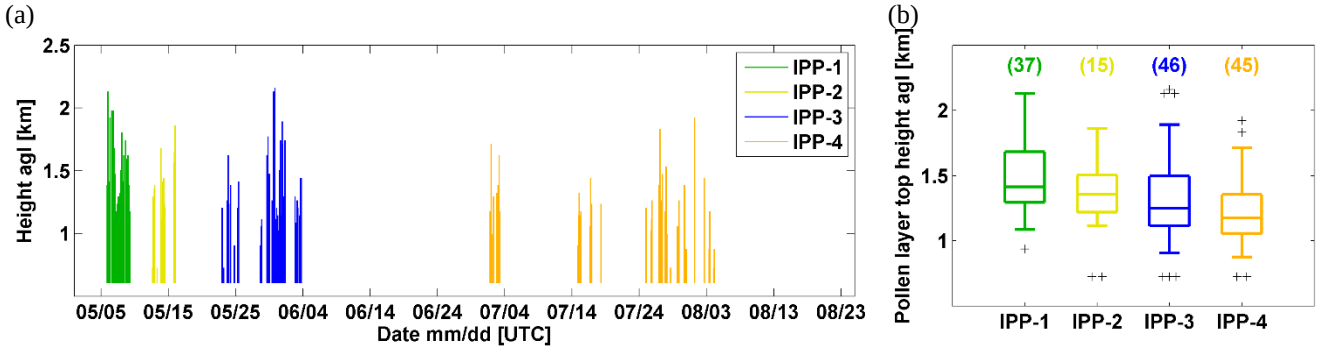

Figure 2. (a) Pollen layer definition for four intense pollination periods (IPPs). (b) Boxplot of pollen layer top heights during each IPP. Number of available profiles are given. Colours are related to the IPPs.

https://doi.org/10.5194/acp-2020-794
Preprint. Discussion started: 6 August 2020

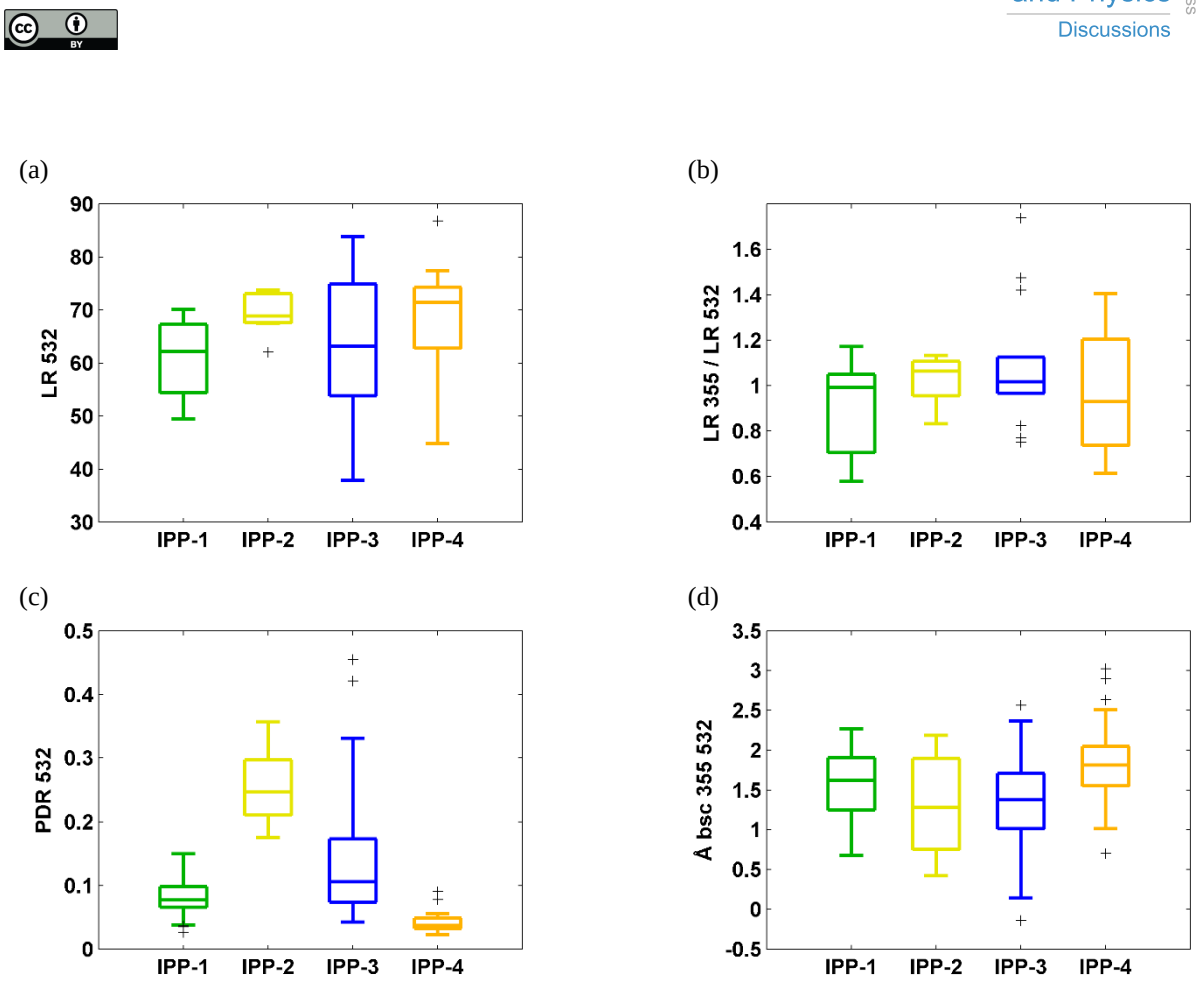

Figure 3. Boxplots of (a) lidar ratio (LR) at 532 nm, (b) ratio of LR at 355 nm and LR at 532 nm during night-time measurements. Boxplots of (c) particle depolarization ratio, and (c) backscatter-related Ångström exponent between 355 and 532 nm during all-day measurements. Mean values of the detected pollen layer for four IPPs are used. The horizontal line represents the median, the boxes the 25 and 75 % percentiles, the whiskers the standard deviation and the plus signs the outliers.

https://doi.org/10.5194/acp-2020-794
Preprint. Discussion started: 6 August 2020

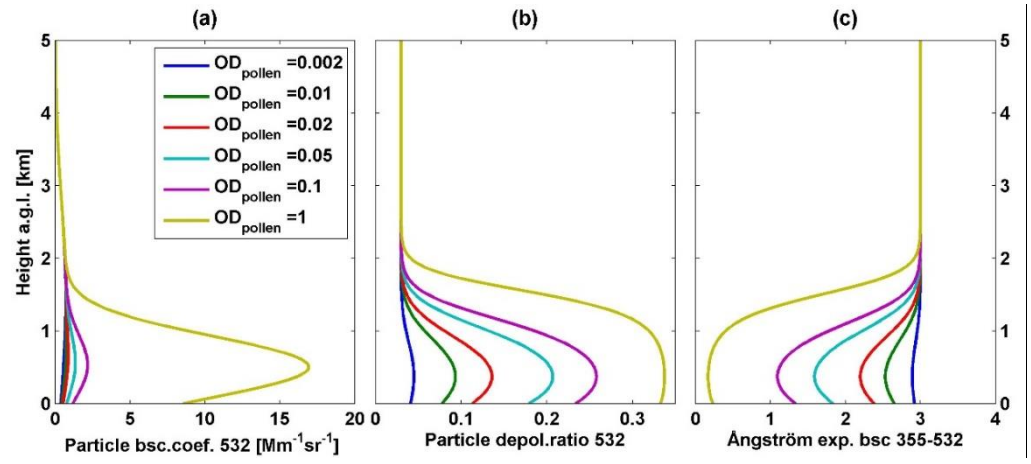

Figure 4. Six cases of simulated vertical profiles of (a) particle backscatter coefficient at 532 nm, (b) particle depolarization ratio at 532 nm, and (c) backscatter-related Ångström exponent between 355 and 532 nm. Simulated results under different input pollen optical depth (OD) values are shown by colour.

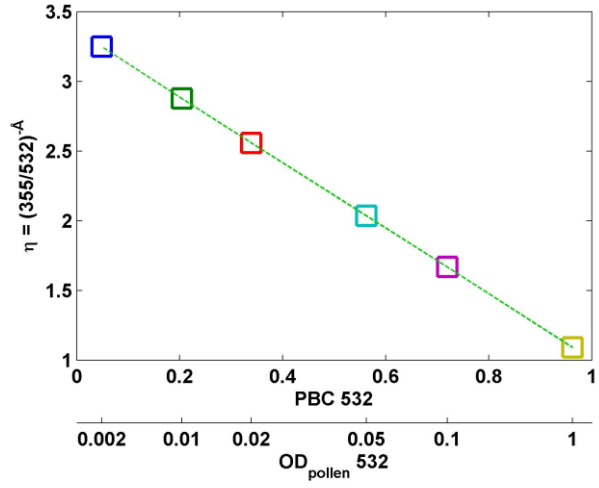

Figure 5. Scatter plot using the η =(355/532)$^{-Å}$ and pollen backscatter contribution (PBC) at 532 nm for 6 simulated cases, of which the input values of pollen optical depth (OD_{pollen}) at 532 nm are defined as 0.002, 0.01, 0.02, 0.05, 0.1, and 1 (shown as the bottom x-axis), and input value of background optical depth is fixed to be 0.1. Mean values of pollen layers (0-1 km) are used for PBC and η.

https://doi.org/10.5194/acp-2020-794
Preprint. Discussion started: 6 August 2020

Atmospheric Chemistry and Physics Discussions

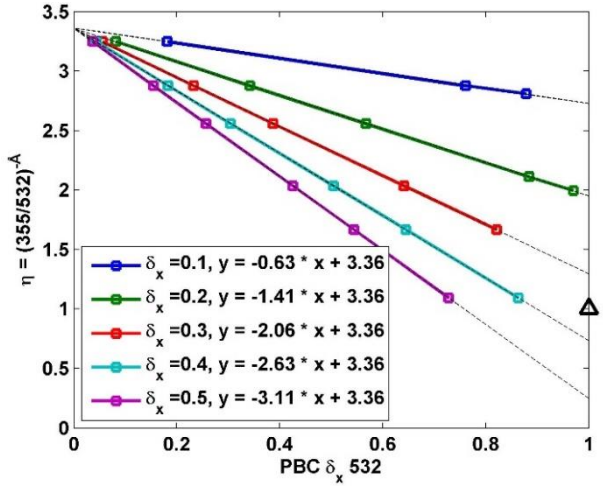

Figure 6. Scatter plots of mean values of η and PBC_{δ_x} in pollen layer under 5 assumed δ_x values cases. η is a parameter using backscatter-related Ångström exponent between 355 and 532 nm (Eq.3), and PBC_{δ_x} is the pollen backscatter contribution at 532 nm inside the pollen layer under a certain assumed pollen depolarization ratio value (δ_x is 0.1, 0.2, 0.3, 0.4, or 0.5). Linear regression lines are drawn by black dotted lines with fitting equation shown. The black triangle shows the ideal value: when PBC is 1, η should be 1 (Å=0).

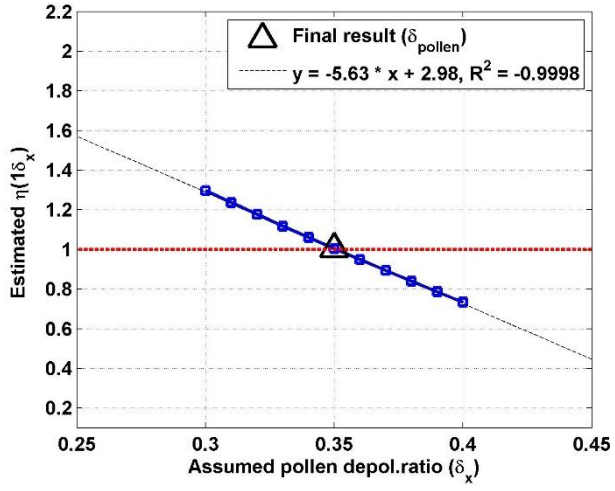

Figure 7. Estimated parameter $\hat{\eta}(\mathbf{1}_{\delta_x})$ against the related assumed pollen depolarization ratio δ_x at 532 nm. Linear regression line is drawn by black dotted line, with fitting equation shown. The correlation coefficient (R^2) value is also given. The final result of 0.35 for pure pollen is found, resulting in $\hat{\eta}(\mathbf{1}_{\delta_x})$=1 (by the black triangle).

https://doi.org/10.5194/acp-2020-794
Preprint. Discussion started: 6 August 2020

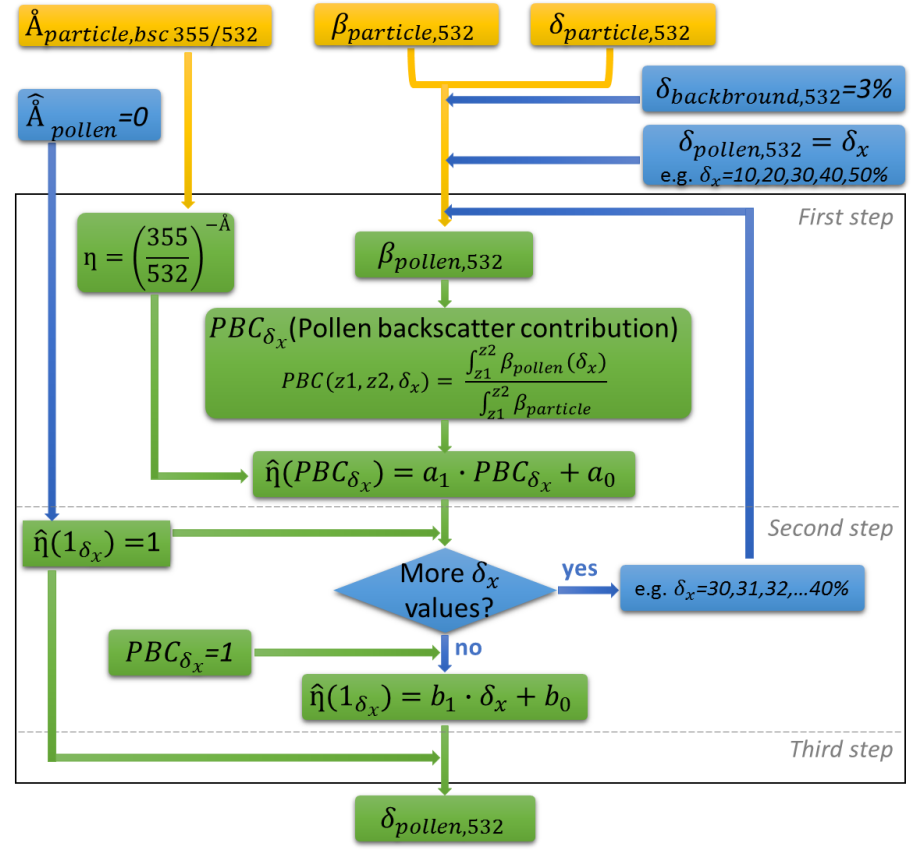

Figure 8. Flow chart of the inverse model for the retrieval of depolarization ratio value for pure pollen. The orange boxes are for the measured parameters (or simulated output from the direct model), blue boxes for the assumptions/manual input and the green boxes for the estimations/calculations. Detail description is in Sect. 3.3.2.

5

https://doi.org/10.5194/acp-2020-794
Preprint. Discussion started: 6 August 2020

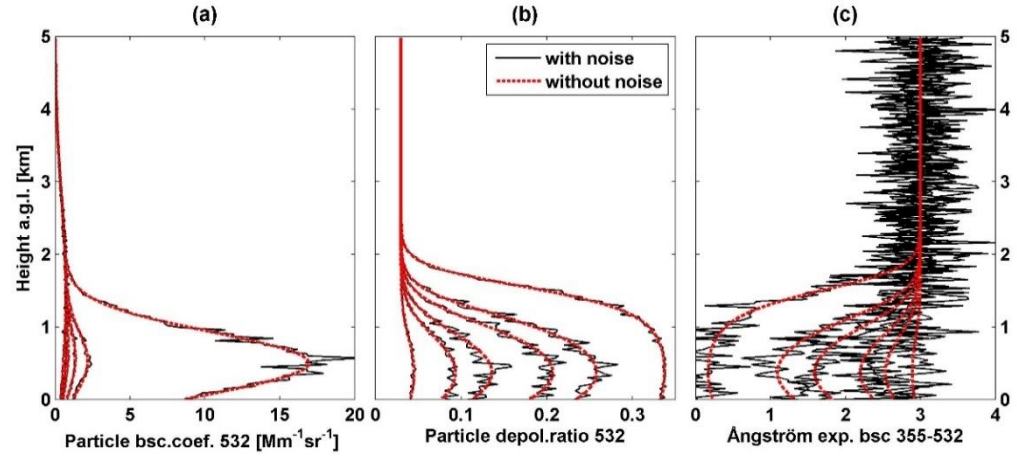

Figure 9. Example of one group of six simulated profiles of (a) particle backscatter coefficient at 532 nm, (b) particle depolarization ratio at 532 nm, and (c) backscatter-related Ångström exponent between 355 and 532 nm. Profiles without noise are shown in red dashed lines, and ones with noise are shown in black lines. Noise levels on backscatter at both 355 and 532 nm were settled as 10 %. Simulated results under 6 input pollen optical depth (OD) values of 0.002, 0.01, 0.02, 0.05, 0.1, and 1 (same as Fig. 4).

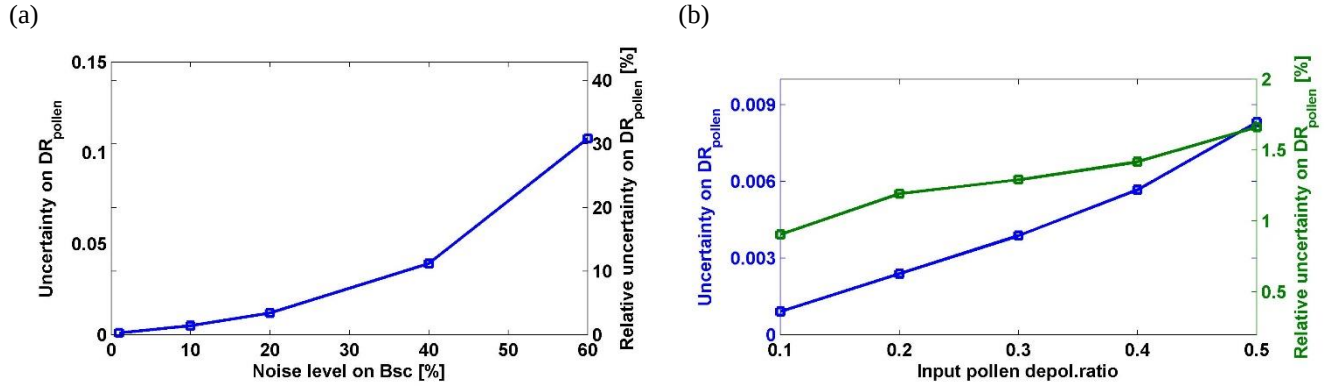

Figure 10. Examples of estimated uncertainties (left y-axis) and relative uncertainties (right y-axis) on retrieved pollen depolarization ratio (DR_{pollen}) at 532 nm against (a) the applied noise levels on backscatter coefficient (Bsc), and (b) the initial input values of DR_{pollen}, using Monte Carlo method. The initial input value of DR_{pollen} is 0.35 for the example in (a). The noise level on backscatter coefficient (Bsc) is 10% for the example in (b).

https://doi.org/10.5194/acp-2020-794
Preprint. Discussion started: 6 August 2020

Atmospheric Chemistry and Physics Discussions

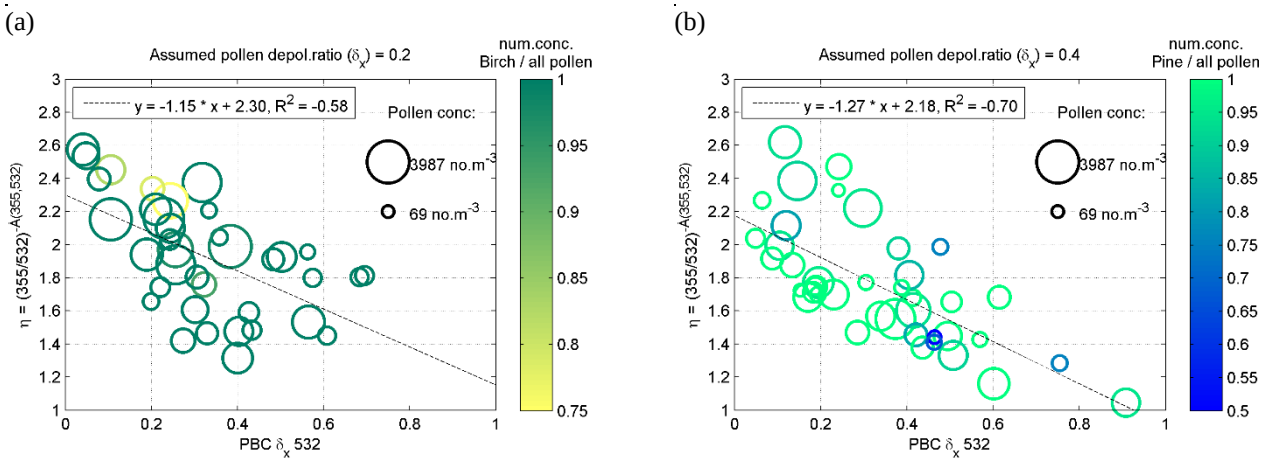

Figure 11. Mean values of the parameter η against pollen backscatter contribution (PBC) at 532 nm inside the pollen layers, during the IPP-1 (a) and IPP-3 (b). η is a parameter using backscatter-related Ångström exponent between 355 and 532 nm (Eq.3). The pollen depolarization ratio δ_x at 532 nm is assumed to be 20% for (a) or 40% for (b). Linear regression lines are drawn by dotted lines, with fitting equation shown. The correlation coefficient (R^2) is also given. The size denotes the total pollen concentrations measured by the Burkard sampler on roof level; the colour represents the number concentration of the dominant pollen (a: birch, b: pine) against the total pollen number concentration. Similar figures using different assumed values of pollen depolarization ratio can be found in Fig. S4 and Fig. S5.

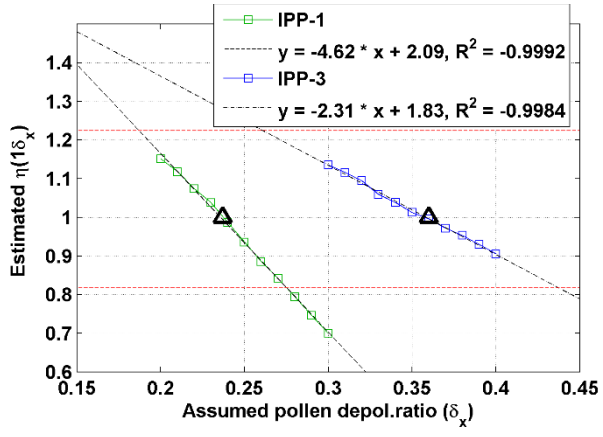

Figure 12. Estimated $\hat{\eta}(\mathbf{1}_{\delta_x})$ against the related assumed pollen depolarization ratio δ_x at 532 nm for IPP-1 (in green) and IPP-3 (in blue). Linear regression lines are drawn by dotted lines, with fitting equations shown. The correlation coefficient (R^2) values are also given. η is a parameter using backscatter-related Ångström exponent between 355 and 532 nm (Eq.3), and $\hat{\eta}(\mathbf{1}_{\delta_x})$ is the estimated $\hat{\eta}$ value for PBC_{δ_x}=1 (Eq.7). The final results for pure pollen are shown by the black triangles. $\hat{\eta}$ values of 0.82 and 1.22 (i.e. Ångström exponent of -0.5 and 0.5) are shown by red dotted lines.

https://doi.org/10.5194/acp-2020-794
Preprint. Discussion started: 6 August 2020

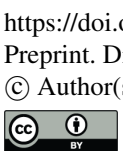

Atmospheric Chemistry and Physics Discussions

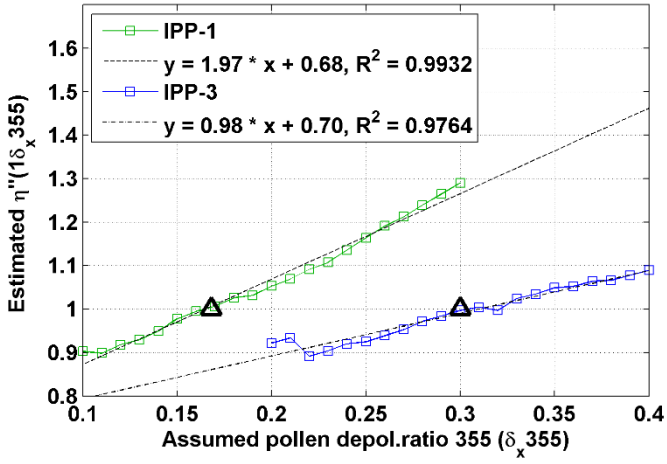

Figure 13. Estimated $\widehat{\eta''}(\mathbf{1}_{\delta_x,355})$ against the related assumed pollen depolarization ratio δ_x at 355 nm for IPP-1 (in green) and IPP-3 (in blue). Linear regression lines are drawn by dotted lines, with fitting equations shown. The correlation coefficient (R^2) values are also given. η'' is a parameter using backscatter-related Ångström exponent between 355 and 532 nm (Eq.9), and $\widehat{\eta''}(\mathbf{1}_{\delta_x,355})$ is the estimated $\widehat{\eta''}$ value for $PBC_{\delta_x,355}$=1. The final results for pure pollen are shown by the black triangles. Results are under the assumption that the backscatter-related Ångström exponent between 355 and 532 nm for pure pollen is 0.

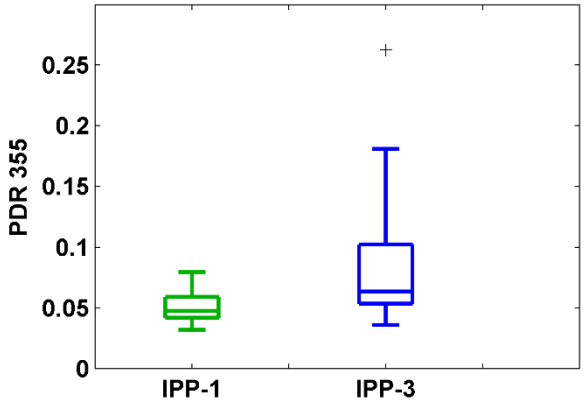

Figure 14. Boxplots of estimated particle depolarization ratio at 355 nm. Mean values of the detected pollen layer for every IPPs are used. The horizontal line represent the median, the boxes the 25 and 75 % percentiles, the whiskers the standard deviation and the plus signs the outliers. Results are under the assumption that the backscatter-related Ångström exponent between 355 and 532 nm for pure pollen is 0.

https://doi.org/10.5194/acp-2020-794
Preprint. Discussion started: 6 August 2020

Atmospheric Chemistry and Physics Discussions

Table 1. (a) Dominant pollen types with their pollen season period, Latin name (Taxa), and typical size. (b) Selected intense pollination periods (IPPs) and the presented dominant pollen types during each IPP. See more descriptions in Sect. 3.1.

(a) ***Dominant pollen types***			
Pollen type	**Pollen season (mm.dd – mm.dd)**	**Taxa**	**The longest axis size (µm)***
Birch	04.29-05.26	*Betula*	22 - 28
Spruce	05.13-06.14	*Picea*	90 - 110
Pine	05.23-06.13	*Pinus*	65 - 80
Nettle	06.27-08.14	*Urtica*	15 - 20
(b) ***Selected intense pollination periods (IPPs)***			
IPP	**Period time (mm.dd – mm.dd)**	**Pollen types (percentage of number concentration)**	
IPP-1	05.05-05.09	Birch (97%), other pollen (3%)	
IPP-2	05.12-05.16	Birch (82%), Spruce (14%), other pollen (4%)	
IPP-3	05.23-05.25 & 05.28-06.03	Pine (95%), other pollen (5%)	
IPP-4	07.01-07.03 & 07.14-07.18 & 07.24-08.04	Nettle (75%), other pollen (25%)	

* Values from Nilsson et al., 1977.

Table 2. Lidar derived optical values of pollen layer for the intense pollination periods (IPPs) (mean values ± standard derivation are given). LR: lidar ratio, PDR: particle depolarization ratio, Å bsc: backscatter-related Ångström exponent.

	Raman cases	LR 355nm [sr]	LR 532nm [sr]	All cases	PDR 532nm	Å bsc 355nm-532nm
IPP-1	10	54 ± 12	61 ± 8	37	8 ± 3 %	1.57 ± 0.43
IPP-2	7	71 ± 10	69 ± 4	15	25 ± 6 %	1.32 ± 0.61
IPP-3	13	66 ± 12	63 ± 14	46	14 ± 9 %	1.38 ± 0.57
IPP-4	15	63 ± 14	68 ± 11	45	4 ± 1 %	1.83 ± 0.43

Table 3. Parameters of pollen and background aerosol layers as input of the direct model. LR: lidar ratio, DR: depolarization ratio, Å bsc: backscatter-related Ångström exponent. A Gaussian distribution is applied for each layer with layer center and half width given.

Aerosol type	LR 355nm [sr]	LR 532nm [sr]	DR 355nm	DR 532nm	Å bsc 355-532nm	Layer center	half width (Gauss)
Pollen	65	65	0.35	0.35	0	0.5 km	1 km
Background	50	50	0.03	0.03	3	1.5 km	3 km

https://doi.org/10.5194/acp-2020-794
Preprint. Discussion started: 6 August 2020

Atmospheric Chemistry and Physics Discussions

Table 4. Depolarization ratios for pure pollen. The assumption of backscatter-related Ångström exponent between 355 and 532 nm should be 0 ± 0.5 was applied for this study. See more details in Sect. 3.4.

	Pollen type	Depolarization ratio at 532 nm	Depolarization ratio at 355 nm
This study, Finland	Silver birch	24 ± 3 %	17 %
(in the atmosphere)	Scots pine	36 ± 5 %	30 %
Cao et al. (2010), Canada	Paper birch	33 %	8 %
(in an aerosol chamber)	Virginia pine	41 %	20 %